Article:
Wang, F, Shen, Y, Huang, Q et al. (3 more authors) (2015) Efficient RNA delivery by integrin-targeted glutathione responsive polyethyleneimine capped gold nanorods. Acta Biomaterialia, 23. 136 - 146 (11). ISSN 1742-7061

https://doi.org/10.1016/j.actbio.2015.05.028

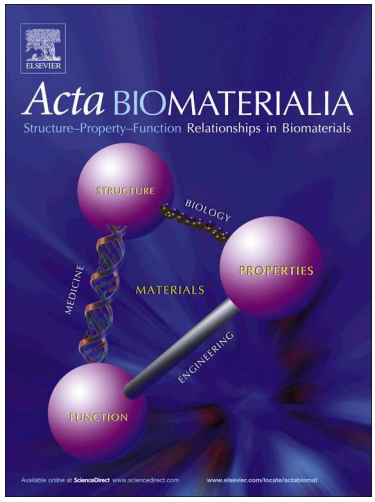

Efficient RNA delivery by integrin-targeted glutathione responsive polyethyleneimine capped gold nanorods

Feihu Wang, Wenjun Zhang, Yuanyuan Shen, Qian Huang, Dejian Zhou, Shengrong Guo

PII: S1742-7061(15)00252-4
DOI: http://dx.doi.org/10.1016/j.actbio.2015.05.028
Reference: ACTBIO 3721

To appear in: *Acta Biomaterialia*

Received Date: 6 February 2015
Revised Date: 29 April 2015
Accepted Date: 22 May 2015

Please cite this article as: Wang, F., Zhang, W., Shen, Y., Huang, Q., Zhou, D., Guo, S., Efficient RNA delivery by integrin-targeted glutathione responsive polyethyleneimine capped gold nanorods, *Acta Biomaterialia* (2015), doi: http://dx.doi.org/10.1016/j.actbio.2015.05.028

Efficient RNA delivery by integrin-targeted glutathione responsive polyethyleneimine capped gold nanorods

Feihu Wang [a,b], Wenjun Zhang [a], Yuanyuan Shen [a], Qian Huang [a], Dejian Zhou [c] *, Shengrong Guo [a,c] **

[a] School of Pharmacy, Shanghai Jiao Tong University, 800 Dongchuan Road, Shanghai 200240, PR China

[b] Shanghai Institute of Pharmaceutical Industry, 1111 Zhongshan Beiyi Road, Shanghai 200437, PR China

[c] School of Chemistry, Astbury Centre for Structural Molecular Biology, University of Leeds, Leeds LS2 9JT, UK

** Corresponding to: Shengrong Guo, School of Chemistry, Astbury Centre for Structural Molecular Biology, University of Leeds, Leeds LS2 9JT, UK. Tel./fax: +44-7459025683.

E-mail address: srguo@sjtu.edu.cn (S. Guo), d.zhou@leeds.ac.uk (D. Zhou).

Abstract

RNA interference (RNAi) mediated gene silencing holds significant promises in gene therapy. A major obstacle to efficient RNAi is the systemic delivery of the therapeutic RNAs into the cytoplasmon whithout being trapped in intracellular endo-/lyso-somes. Herein we report the development of a PEGylated, RGD peptide modified, and disulfide cross-linked short polyethylenimines (DSPEIs) functionalized gold nanorod (RDG) for targeted small hairpin (sh)RNA delivery. The RDG effectively condensed shRNAs into stable nanoparticles, allowing for highly specific targeting of model human brain cancer cells (U-87 MG-GFP) via the $\alpha_v\beta_3$ integrins-mediated endocytosis. The combined effects of endosomal escape (via the proton-sponge effect of the PEIs) and efficient cleavage of the disulfide-cross-linked DSPEIs by the high intracellular glutathione content triggered rapid cytoplasma shRNAs release resulted in excellent RNAi efficiency and low cytotoxicity. Furthermore, the high stability and prolonged blood circulation afforded by PEGylation allowed for highly effective, targeted tumor accumulation and internalization of the carriers, resulting in outstanding intra-tumor gene silencing efficiency in U-87 MG-GFP tumor bearing BALB/c mice. Combining the capabilities of both passive and active targeting, intracellular glutathione-triggered "off-on" release and endosomal escape, the RDG nanocarrier developed herein appears to be a highly promising non-viral vector for efficient RNAi.

Keywords: Gold nanorods, Disulfide-linked polyethylenimine, Glutathione, RGD peptide, RNA delivery

1. Introduction

RNA interference (RNAi) has been proven to be a useful approach to treat various genetic diseases. It can down-regulate specific protein expression by silencing the activity of its targeted gene [1-5]. This approach exhibits significant promises for the development of a new class of molecular therapeutic drugs that interferes with disease-causing or –promoting genes, particularly those that encode so-called "non-druggable" targets not amenable to conventional therapeutics [6, 7]. However, many natural obstacles have to be overcome to achieve safe and efficient *in vivo* delivery of therapeutic RNAs [8-11]. Thus, realizing the full potential of the RNAi-based therapeutics requires the development of an ideal carrier [4, 12-15] that should be able to bind and condense RNA, provide protection against enzymatic degradation, selectively deliver RNA to target tissues, facilitate its intracellular uptake and escape from the endosome/lysosome, "on demand" RNA release, and finally promote efficient gene silencing [2, 16-18].

In recent years, gold nanorods (GNRs) have attracted considerable attention for their unique properties in localized photothermal therapy [19, 20], biosensing [21], and molecular imaging [22]. Particularly, being an anisotropic, rod-shaped nanomaterial that is easily functionalized, GNR has begun to attract significant research interest in gene delivery [7, 23-26]. Currently, two main strategies in GNR based gene delivery have been investigated: one is to use GNR as an active carrier where its photothermal properties are harnessed to selectively release the gene in a localized area. [23, 24, 26]. Another approach is the use of layer-by-layer (LBL) technique where biocompatible polymers or proteins (such as polyacrylic acid (PAA), polystyrenesulfonate (PSS) or bovine serum albumin (BSA)) are first over-coated on the CTAB-capped GNR surface, which is then functionalized with a layer of cationic polymer (such as polyethylenimine (PEI)) to switch GNR net surface charge to positive. The resulting carrier is used for gene condensation and subsequent intracellular gene delivery [27-30].

Although these two strategies can achieve laser-triggered gene release and/or reduced toxicity, they both have their own disadvantages. The first strategy cannot provide protection of the gene against degradation and the photothermal effect of GNR may cause cell death [23]. The limitation of the second strategy is that the carrier exhibited lower transfection efficiency than that of PEI/DNA complexes [27]. More recently, Ryan and co-worker have explored a poly-L-lysine peptide (PLL) capped gold nanoshell (GNS) for therapeutic oligonucleotide delivery and Cui's group has developed a RGD-conjugated dendrimer-modified GNR for gene delivery [7, 25]. Both approaches exhibit controlled gene release and improved delivery efficiency with low

toxicity. Therefore, developing a "fine-tuned" surface for GNR is critical to improve its biocompatibility and application in gene/RNA delivery.

Polyethylenimine (PEI) has been regarded as the "gold" standard for gene delivery because it shows relatively high transfection efficiency due to its proton sponge effect and ability to protect DNA from enzymatic degradation [31, 32]. High molecular weight PEIs (such as 25-kDa PEI) are highly effective in gene transfection, but also have high cytotoxicity due to the high cationic density and lack of biodegradability [33]. Low molecular weight PEIs(such as 1.8-kDa PEI) have much lower cytotoxicity, but they cannot effectively condense DNA and display very poor gene transfection activity [33, 34]. In order to reduce the cytotoxicity and enhance carrier unpacking into the cytosol and/or nucleus, intracellular-cleavable disulfide-linked PEIs have been designed for gene delivery [35-39]. The disulfide linkage is stable during blood circulation [40]. Once inside cells, the cross-linking disulfide bonds are cleaved under the high concentration of reductive glutathione (GSH), making it favorable to unpack the PEI shell and release the infective nucleic acids [33, 41]. Therefore, a cleavable disulfide cross-linked PEI (DSPEI) was synthesized as the gene/RNA carrier with controlled-release property in response to intracellular reducing environments.

Integrin $\alpha_v\beta_3$, an important biomarker often over-expressed on actively angiogenic endothelium and malignant glioma cell surfaces, plays a critical role in regulating tumor growth, metastasis and tumor angiogenesis [42, 43]. The cyclic RGD (arginine-glycine- aspartic acid) peptide (cRGD) can specifically bind with integrin $\alpha_v\beta_3$ [42, 44]. The high affinity interaction between the RGD peptide and over-expressed integrins on cancer cell surfaces has led to a widespread use of RGD peptide as ligand for integrin-targeted drug and gene delivery [44-46]. Thus, we have selected the RGD peptide as the targeting molecules for specific glioblastoma cell therapy.

We have recently developed an effective intracellular gene delivery system, RDG (RGD-PEG-DSPEI-GNR) that combine the advantageous properties of RGD-mediated specific targeting and intracellular stimuli-triggered degradability of DSPEI. This gene nanocarrier exhibited high transfection efficiency with low cytotoxicity. Herein, we report that the RDG could be used for targeted and intracellular small hairpin (sh)RNA delivery for effective RNAi therapy. The GSH triggered shRNA release, gene silencing efficiency and cytotoxcity of the RDG/shRNA complex nanoparticles were investigated at both cellular level and also *in vivo* mouse model using U-87 MG cells and tumor-bearing mice.

2. Materials and methods

2.1. Materials

RDG (RGD-PEG-DSPEI-GNR), DG (DSPEI-GNR) and RPG (RGD-PEI-25 KDa-GNR) conjugates were prepared in our lab as described previously [47]. Polyethylenimine branched (PEI-25 KDa), L-glutathione (Reduced) (GSH), glutathione reduced ethyl ester (GSH-OEt), 3-(4, 5-dimethylthiazol-2-yl)-2,5-diphenyltetrazolium bromide (MTT), ethidium bromide (EB), bisBenzimide H 33342 trihydrochloride (Hochest 33342) and trypan blue were obtained from Sigma Co., Ltd. (USA). YOYO-1 and Lyso Traker Red were obtained from Invitrogen Molecular Probes (USA). Tissue Freezing Medium (OCT) was purchased from Leica (Germany). Hydrochloric acid (HCl, 36.0~38.0 wt % in water) and nitric acid (HNO_3) were obtained from Sinopharm chemical Reagent Co., Ltd. (China). The Dulbecco's modified Eagle medium (DMEM), penicillin–streptomycin, fetal bovine serum (FBS), 0.25% (w/v) trypsin–0.03% (w/v) EDTA solution and Phosphate buffer solution (PBS) were purchased from Gibco BRL (USA). Water was purified by distillation, deionization, and reverse osmosis (Milli-Q plus). All reagents were analytical grades and used without further purification.

The pGPU6/Neo-GFP22-shRNA-expressing pDNA that targets the sequence GCAGCACGACTTCTTCAAG was obtained from GenePharm Co. Ltd. (Shanghai, China) and purified with the Plasmid Maxi Kit (Qiagen GmbH, Hilden, Germany) in accordance with the manufacturer's instructions. The concentration of plasmid solution was determined by measuring the ultraviolet (UV) absorbance at 260 nm and the ratio of its optical density at 260 nm to 280 nm was in the range of 1.8 to 1.9.

2.2. Cell culture

The U-87 MG (human glioblastoma cell) cell line was generously donated by School of Pharmacy, Fudan University. The U-87 MG cells expressing stable enhanced green fluorescence protein (U-87 MG-GFP cells) were kindly provided by Center of Pharmaceutics, Shanghai Institute of Materia Medica. GFP-negative cells were cultured in DMEM containing 10% fetal bovine serum (FBS), 100 Units/mL penicillin G sodium and 100 μg/mL streptomycin sulfate (complete DMEM medium). GFP-positive cells were grown in complete DMEM medium with 50 μg/mL G418. Cells were maintained at 37 ℃ in a humidified and 5% CO_2 incubator. Cells grown to confluence were subcultured every other day after trypsinized with 0.25% trypsin–EDTA and diluted (1/3) in fresh growth medium.

2.3. Animals

Male BALB/c mice aged 6 weeks (20–25 g) obtained from the Experimental Animal Center of Fudan University (Shanghai, China) and kept under a 12 h light/dark cycle at the Animal Care Facility with food and

water *ad libitum*. The animals were acclimatized to the laboratory environment for at least 5 days prior to the experiments. All experiments were performed in accordance with the Animal Care and Welfare Committee of Fudan University and followed the animal care guidelines of the National Institutes of Health.

2.4. Preparation and characterization of RDGNR/shRNA complex nanoparticles

RGD peptide modified disulfide cross-linked polyethylenimine (DSPEI) capped GNR (RDG) was prepared according to our previous report[47]. The RDG/shRNA complex nanoparticles were prepared at seven different mass ratios ranging from 1 to 15 between the GNR nanocarriers and the GFP-shRNA. Briefly, various amount of RDG in water was added into the same volume of shRNA (50 μg/mL in water). The mixture was then vortexed for 30 s and incubated at room temperature for 30 min.

The shRNA binding ability of the RDG nanocarriers was confirmed by agarose gel electrophoresis. The RDG-based complexes containing 0.5 μg of shRNA at various mass ratios were loaded on 1% agarose gel in TAE buffer (40 mM Tris–HCl, 1 v/v% acetic acid, and 1 mM EDTA) containing 0.5 μg/ mL EB and subjected to electrophoresis with a current of 100 V for 50 min. The resulting shRNA bands were visualized with a UV (254 nm) illuminator and photographed with a Vilber Lourmat imaging system.

For quantification of shRNA binding efficiency by the RDG nano-carrier, shRNA was fluorescently labeled with a nucleic acid stain YOYO-1 (excitation wavelength: 491 nm, emission wavelengths: 509nm) by mixing shRNA and YOYO-1 with a ratio of 1.5 nanomole dye molecule/100μg shRNA and incubated for 30 min at room temperature in the dark. The RDG/YOYO-1-labeled shRNA complexes were prepared and incubated at 37 ℃ for 30 min. Afterwards, the samples were centrifuged to remove the GNRs and collect the supernatants. Fluorescence spectrophotometer (F-7000, Hitachi, Japan) was used to quantify the unbound shRNA in supernatants.

The zeta-potential of RDG/shRNA complexes were measured with Zetasizer NanoZS/ZEN3600 (Malvern Instruments, Herrenberg, Germany). The morphology and size of complexes were observed using a transmission electron microscope (TEM) (JEM-2100F, JEOL, Japan).

2.5. In vitro GSH triggered release studies

The GSH triggered reductive degradation of RDG-based complexes was also evaluated by agarose gel electrophoresis. RDG/shRNA complexes at different mass ratios were prepared as described above. After incubation for 30 min, GSH was added directly into the nanoparticle solution to reach a final concentration of 3 mM, which was comparable to the intracellular environment [48]. The nanoparticle solution was incubated at 37 ℃ for 30 min before agarose gel electrophoresis. For quantification of GSH triggered gene release from

RDG/shRNA complexes, the RDG/YOYO-1-labeled shRNA complexes were prepared and treated with GSH at a concentration of 3 mM at 37 ℃ for 30 min. Afterwards, the samples were immediately centrifuged to remove the GNRs and collect the supernatants. Fluorescence spectrophotometer (F-7000, Hitachi, Japan) was used to quantify the released shRNA in supernatants. We quantified the fluorescence intensity of YOYO-1 due to YOYO-1-labeled shRNA released from RDG-based complexes.

2.6. Cell targeting of RDG/shRNA complex

The MCF-7 cell line with lower expression of $\alpha_v\beta_3$ was selected as the negative control group. The human glioblastoma U-87 MG-GFP cell line with over-expression of $\alpha_v\beta_3$ was selected as test group. The cells were seeded onto 20 mm glass coverslips in a 12-well tissue culture plate at a density of 2×10^5 cells per well and incubated with GNR-based complexes with shRNA concentration of 2.5 μg/well in the culture medium for 2 h to allow cellular uptake. For comparison, DG/shRNA complex nanoparticles were performed as a positive control. In the free RGD peptide competition study, 1 μM RGD peptide was added to the incubation medium. After incubation, the cells were washed with PBS solution and fixed with 4% paraformaldehyde solution in PBS for 30 min, then the fixed cells were washed with PBS and sealed with slide. The light scattering images were recorded by using a dark-field microscope (Olympus IX71, Olympus, Japan) with an EMCCD camera (Cascade 128+, Roper Scientific, Inc.). For quantification of GNRs uptaken in cells, inductively coupled plasma mass spectroscopy (ICP-MS) measurements were performed. After a 2 h incubation, the media was aspirated off, the cells were washed with PBS. Live cells were sorted and counted using flow cytometry and digested with aqua regia, and then the gold content was measured with the ICP-MS (7500A, Agilent, USA). The amount of GNRs was finally normalized to the cell number.

The GNR number per cell was estimated as follows: the volume of one GNR, assuming 50 nm for the length and 10 nm for the diameter (based on TEM images), is $V=\pi r^2 l = \pi \times (6\ nm)^2 \times 50\ nm$ = 5652 nm^3, which means that the theoretical average mass per GNR (M_{GNR}) is 1.09×10^{-16} g (ρ_{Au} = 19 300 kg m^{-3}). Flow cytometry gives a specific number of cells (N_{cells}). ICP-MS was used to quantify grams of gold (M_{Au}). The number of GNRs per cell was then calculated:

$$GNRs/Cell = \frac{M_{Au}}{M_{GNR} \times N_{Cells}}$$

2.7. Intracellular GSH-triggered shRNA release

U-87 MG cells were first added into a 12 well-plate at a cell density of 1×10^5 per well. After overnight incubation, 10 mM GSH-OEt was pre-treated for 2 h followed by the incubation of the cells with RDG/YOYO-1-labeled shRNA complexes (prepared at a mass ratio of 5 with shRNA concentration of 2.5

μg/well) for 3 h. The cells were then washed by PBS, trypsinized and resuspended in the medium. Subsequently, the fluorescence intensity was analyzed and quantified using flow cytometry (BD LSRFortessa, Becton Dickinson, USA). The data shown are the mean fluorescent signals for 10,000 cells. For comparison, RPG/shRNA complexes nanoparticles were performed as a positive control.

2.8. CLSM studies

Cell uptake and intracellular shRNA release of RDG/shRNA complexes was further analyzed by CLSM studies. U-87 MG cells were seeded at a density of 1×10^5 cells/well onto glass coverslips in a 12-well plate and allowed to attach for 24 h. Followed by removing the complete medium, the cells were incubated with the same reagents in intracellular GSH-triggered shRNA release studies. Then, the medium was aspirated, the cells were washed twice with PBS and treated with Hoechst 33342 (6 μg/mL) and Lyso Tracker Red DND-99 (10 nmol/mL) at 37 ℃ for additional 20 min [49]. The extracellular fluorescence was quenched with 500 μL of 0.4% trypan blue for 2 min. Followed by completely washing with PBS, the cells on coverslips were fixed with 500 μL of 4% paraformaldehyde for 30 min, then the fixed cells were mounted in anti-fluorescence quenching mounting medium and sealed with slides. Cells were visualized under a confocal laser scanning microscope (CLSM) (TCS SP5, Leica, Germany) to observe the intracellular distribution of the YOYO-1 labeled shRNA.

2.9. In vitro RNAi and cell viability assays

RNAi experiment was performed with U-87 MG-GFP cells by using the GFP-shRNA as reporter gene. For silencing experiment, the cells were seeded at a density of 1×10^5 cells/well in a 12-well plate and allowed to attach for 24 h prior to transfection. Then, the media was replaced with fresh medium containing RDG/shRNA complexes with 2.5 μg/well of shRNA, and the cells were incubated for an additional 36 to 48 h. The silencing of GFP was visualized under a fluorescent microscope (Olympus IX51, Olympus, Japan). The GFP-negative cells and relative light units (RLUs) were quantified by flow cytometry (BD LSRFortessa, Becton Dickinson, USA). The total protein was measured according to a BCA protein assay kit (Pierce). GFP silencing activity was expressed as RLU/mg protein. For comparison, DG/shRNA prepared at a mass ratio of 5 and PEI-25 kDa/shRNA complexes with N/P ratio of 10 were performed as positive controls. For each formulation, the cells were transfected in triplicates.

To evaluate the cytotoxicity of the vector, cells were seeded in 96-well plates at a density of 5×10^3 cells per well and allowed to attach overnight. After the medium was aspirated, the cells were treated with RDG at a concentration of 1, 5, 25, 50 and 75 μg/ml, PEI 25-kDa at the concentration of 3.9 μg/ml (the concentration of PEI 25-kDa at N/P ratio of 10) was used as a positive control. Followed by incubation for 48 h, the MTT assay

was performed. Briefly, 20 μl of 5 mg/ml MTT dissolved in PBS was added to each well. The cells were incubated for an additional 4 h at 37 ℃ and then the medium was discarded. Thereafter, 250 μl of DMSO was added to each well to dissolve the formazan crystals. The absorbance was read on a microplate reader (Bio-Rad 680, USA) at a test wavelength of 570 nm and reference wavelength of 630 nm. The percentage of cell growth inhibition was calculated as follows: inhibitory rate = ($A570_{control} - A570_{sample}$)/$A570_{control}$ × 100%.

To obtain a more convincing data about the cytotoxicity of RDG, cell viability was determined after the cells were treated with RDG/shRNA complex nanoparticles. Complexes with shRNA concentration of 3 μg/mL at mass ratio of 10, 7.5 and 5 were added into the cells. MTT assays were performed similarly to the experiments mentioned above. RPG/shRNA complex at mass ratio of 5 and PEI/shRNA complex at N/P ratio of 10 were also used as control.

2.10. In vivo biodistribution and RNAi experiment

Subcutaneous tumors on the left flank of male nude mice were initiated by the injection of 2×10^6 viable U-87 MG-GFP cells in a volume of 0.2 mL. Tumors were allowed to reach about a volume of 150-200 mm^3. Mice were randomly divided into two groups (n=5) and injected through the tail vein with RDG/shRNA and DG/shRNA complexes (both prepared at a mass ratio of 5, shRNA of 2 mg/kg), respectively. To investigate the biodistribution of GNR-based complex nanoparticles, the mice were sacrificed at 12 h after the i.v. injection. The major organs including tumors were collected and completely lysed in aqua regia. Then, the solution was evaporated and suspended in an aqueous solution containing 1.0% aqua regia and the amounts of GNR in tissue samples were measured by ICP-MS (7500A, Agilent, USA).

For *in vivo* RNAi experiment, mice were randomly assigned to experimental and control groups (n=5). Animals were injected through the tail vein with Saline, PEI-25 kDa/shRNA, DG/shRNA, and RDG/shRNA complexes (shRNA of 2 mg/kg), respectively. After 48 h, the mice were sacrificed. The tumors were taken out, washed with cold saline and observed using a Mulaurora™ *in vivo* fluorescence imaging system (ZKKS, China). After which the tumors were imbedded in OCT. The frozen sections of the tumors were prepared and visualized under the fluorescence microscope (Olympus IX51, Olympus, Japan). For quantitative determination of the gene silencing efficiency, the tumors were cut into 1-2 mm^3 pieces and then trypsinized with 0.25% trypsin–EDTA at 37 ℃ for 20 min. The cell suspension were filtered through 74 μm nylon membranes, centrifuged at 1000×g for 5 min, washed twice with PBS and resuspended in 0.5 mL PBS. Then, the silencing efficiency of the cells were quantified by flow cytometry (BD LSRFortessa, Becton Dickinson,USA).

2.11. Statistical analysis

The mean ± SD was determined for each treatment group. Student's *t*-test (two-tailed) or one-way analysis of variance (ANOVA) was applied to evaluate the significance. The statistical significance criterion *P* value was 0.05.

3. Results and discussion

3.1. Characterization of RDG/shRNA complexes

We have recently synthesized a targeted polymeric gene carrier, RD, by incorporating a RGD peptide into the disulfide cross-linked cationic polymer, DSPEI, *via* a hydrophilic polyethylene glycol (PEG) spacer (Fig. S1). The DSPEI with a molecular weight of 22.5 kDa could be degraded under the intracellular reductive environment, but is relatively stable under physiological conditions. Monodisperse GNRs with an aspect ratio of 4.1 were synthesized by using the seed-mediated growth method (Fig. S2A). In order to enhance stability, direct cell-specific targeting and controlled release "cargos" such as genes, the GNR surface was successfully functionalized with RDs via "round-trip" phase transfer ligand exchange (Fig. S3). The phosphotungstic acid negative stained TEM images revealed that the GNRs were coated with a layer of RD conjugates without any shape change (Fig. S2B). The RDG was stable even after 6 months of storage at high concentration (3×10^{-8} M), and the plasmon peaks exhibited no significant changes in peak width or position, suggesting a good long-term stability. Zeta potential measurements further confirmed that the RDG had a high positive charge of 48.7±2.8 mV, indicating it could have a good gene loading capacity.

GNR-based shRNA complexes were prepared by adding the RDG solution into the shRNA solution in equal volumes. The shRNA concentration was kept constant. The concentration of RDG was adjusted according to the desired GNR/DNA mass ratios ranging from 1 to 15.

To be an effective gene vector, cationic polymers must be able to bind and condense shRNA into nanoparticles, which can then be taken up by cells. The shRNA binding and condensation capability of the synthesized RDG were investigated by gel retardation assay and shRNA bound efficiency measurements. As shown in Fig. 1A and B, the RDG conjugates can completely retard shRNA migration and the shRNA nearly completely (98 %) condensed on the RDG nano carrier at a mass ratio of above 3, indicating that RDG exhibited strong capability to condense shRNA. Zeta potentials of the complexes under different mass ratios were measured and shown in Fig. 1C. At a mass ratio of above 3, all the complexes showed positive surface charges, suggesting that they were able to condense shRNA into complexes. The zeta potential of RDG /shRNA complexes showed a strong dependence on the mass ratios and decreased rapidly with the

decreasing mass ratio. At a mass ratio of 5, the complex had a positive zeta potential of around + 20 mV. The complexes were further imaged by TEM after negative staining (Fig. 1D). At pH 7.4 and mass ratio of 5, the DSPEIs and RNAs formed compact complexes of about 2 nm thick closely packed on the GNR surface, most likely due to strong electrostatic attractions between the positively charged polymers and negatively charged RNAs. The morphology and size of the GNR itself did not change during the complexes preparation process.

3.2. In vitro GSH-triggered shRNA release

RNA dissociation is one of the rate-limiting steps during RNA delivery, and the efficiency of dissociation is closely related to the overall efficiency of RNA interference [50]. In our previous report [47], gel permeation chromatography (GPC) traces of DSPEI in the absence and presence of GSH clearly showed that the disulfide cross-linked DSPEIs were responsive to the reducing agent GSH (data not shown here). After incubation with GSH for 1 h at 37 ℃, the average molecular weight of DSPEI decreased from 22.5 kDa to 2.1 kDa, which is very close to *M*w of PEI only (1.8 kDa).

To assess the release of shRNA from RDG/shRNA complexes, the complexes were incubated in PBS (pH 7.4) in the presence of 3 mM GSH, which represented the simulated intracellular reducing environment. GSH-triggered release of shRNA from the disulfide-containing GNR- complexes was visualized by gel electrophoresis (Fig. 2A). Compared with Fig.1A where the complexes were incubated in the extracellular physiological condition, the fluorescence bands clearly showed the presence of free shRNA in the supernatants of the RDG/shRNA complexes after incubation with 3 mM GSH (30 min), indicating that shRNAs were rapidly released. This is presumably due to the cleavage of disulfide bonds of DSPEI under the reductive conditions, producing much smaller PEIs that can no longer condense the RNAs. The shRNA release percentage for the GNR-complexes was further quantitated by fluorescence spectroscopy. As the mass ratio was decreased from 15 to 1.5, the released shRNA percentage was rapidly increased (Fig. 2B). At a mass ratio of 5, the released shRNA was 46.6±3.7% under the above conditions. This result indicates that the complexes would be degraded after being internalized into the reductive intracellular environment and release their cargo efficiently. The RDG/shRNA complexes prepared at a mass ratio of 5 not only exhibited desirable shRNA binding and condensation ability, but also favorable shRNA release property upon GSH-stimulation, therefore, the mass ratio of 5 was chosen for the following assays.

3.3. Cell targeting of RGD modified GNR

Two different cell lines, the glioblastoma U-87 MG-GFP cells having over-expressed $\alpha_v\beta_3$ integrins, and the breast cancer cell line MCF-7 cells with low expression of $\alpha_v\beta_3$ integrins were used. To evaluate the specificity

and targeting ability of RGD-modified GNR against $\alpha_v\beta_3$ integrins on the cells, the binding of RDG/shRNA and plain DG/shRNA with U-87 MG-GFP and MCF-7 cells were investigated using dark-field microscopy. As shown in Fig. 3A, the RDG/shRNA incubated MCF-7 cells exhibited a weak golden color, and similar negative result was also observed for DPGNR/shRNA treated U-87 MG-GFP cells. In contrast, the RGD-modified GNRs incubated U-87 MG-GFP cells exhibited a much stronger golden color, suggesting that the RDG/shRNA complex are taken up more efficiently by the U-87 MG-GFP cells, presumably via its surface over-expressed $\alpha_v\beta_3$ integrins. This was supported by incubation of the U-87 MG-GFP cells with RDG/shRNA complex in the presence of 1 mM free RGD peptides led to a significantly reduced cellular uptake of RGD-modified GNRs (Fig. 3Ad). This result suggests that free RGD peptides can inhibit the uptake of the RGD-modified GNR through competitive binding to the tumor cell over-expressed $\alpha_v\beta_3$ integrins, leading to greatly reduced cellular uptake by blocking the effective $\alpha_v\beta_3$ integrins -mediated endocytosis [46, 48, 49].

Furthermore, inductively coupled plasma mass spectrometry (ICP-MS) was used to confirm GNR cellular uptake. By quantifying the GNR number per cell, the highest column in chart shows a significant difference between the RDG/shRNA treated cells and the other three groups (Fig. 3B). The U-87 MG-GFP cell uptake of the RDG/shRNA complex was approximately four-fold higher than that of plain complex, in good agreement with the above imaging results. This result demonstrated that the RGDs on the RDG/shRNA complex were readily accessible to $\alpha_v\beta_3$ integrin binding, and hence the RDG/shRNA complexes can be used as efficient, targeted intracellular gene carriers.

3.4. Intracellular monitoring of the release of shRNA triggered by GSH

It is well known that PEI can protect the gene from lysosomal nuclease degradation and facilitate endosomal escape to the cytoplasm *via* its proton sponge effect [51, 52]. The promotion of the shRNA release from the complexes into the cytoplasm is critical for high gene silencing efficiency. To confirm if the GSH-responsive gene delivery system based on RDG also works in cancer cells, flow cytometry was used to evaluate the release of YOYO-1 labeled shRNA from RDG/shRNA complex within the U-87 MG cells. As shown in Fig. 4A and B, cells treated with RPG/shRNA showed much lower fluorescence compared to RGD-DPGNR/shRNA treated cells. In the case of RPG/shRNA, PEI cannot be degraded within the cell, almost all the fluorescence of YOYO-1 is quenched due to the proximity of the shRNA on the GNR surface [53, 54]. Therefore, a much weaker fluorescence is observed for the RPG/shRNA treated cells. While, the cells incubated with RDG/shRNA complex exhibited much stronger fluorescence, this could be attributed to the dissociation of RDG/shRNA complexes in the reductive intracellular environment, facilitating shRNA release. Glutathione

monoester is rapidly internalized by cells and processed into glutathione (GSH) by esterases [55, 56]. When the cells were pretreated with 10 mM monoethyl ester of GSH (GSH-OEt) for 2 h, a slight fluorescence enhancement was observed for the sample treated with RPG/shRNA, which may be attributed to Au-S bond cleavage between GNR and PEI, leading to a small number of shRNAs being liberated from GNR surface. While, for the RDG/shRNA treated group, the fluorescence profile of YOYO-1 was shifted to the right distinctly and the mean fluorescence intensity was significantly increased after the cells were pre-treated with GSH-OEt. These results clearly prove the intracellular GSH-triggered rapid degradation of disulfide-containing DSPEI and subsequent a significant release of shRNA in the cytosol.

The intracellular shRNA released in response to GSH was also monitored by confocal laser scanning microscopy (CLSM). To trace the intracellular distribution, shRNA was labeled with YOYO-1, Hoechst 33342 and Lyso Tracker Red DND-99 were used for staining the nuclei and lysosomes, respectively. As shown in the CLSM images (Fig. 4C), a few green fluorescent spots were observed in the RDG/shRNA treated U-87 MG cells but the fluorescence intensity is significantly increased after the cells were pretreated with GSH-OEt. Meanwhile, more green fluorescent spots were seen distribution out of lysosomes. These results clearly demonstrate that RDG/shRNA complex nanoparticles could escape from lysosomes and then dissociate and release its shRNA cargo rapidly under reductive intracellular environment.

3.5. In vitro GFP silencing

The *in vitro* RNAi efficiency was detected by model system of shRNA-based reporter GFP knock-down on U-87 MG-GFP cells. Transfection efficiency of RDG based complex was evaluated at a mass ratio of 5, and RPG, DG based complex prepared at mass ratio of 5 and PEI/shRNA complex at N/P ratio of 10 were used as control. All the complex nanoparticles have almost the same surface zeta potential of around +20 mV. For the RNAi experiment, cells were incubated with complexes for 4 h and images were taken after further 42 h culture for GNRs-based complexes and 48 h for PEI/DNA complexes. Fig. 5A depicts green fluorescence of U-87 MG-GFP cells after RNAi qualitatively monitored by fluorescent microscopy. Compared with the untreated cells, the expressed GFP level in U-87 MG-GFP cells was obviously reduced after the cells were treated with the four complex nanoparticles. Cells transfected with DG/shRNA showed comparable GFP intensity with that of RPG/shRNA complexes. Notably, GFP was barely expressed after the cells incubated with RDG/shRNA complexes, which was even less than that of PEI-25 kDa/shRNA complexes group. The GFP silencing activity of shRNA in U-87 MG-GFP cells was further quantified as RLU/mg protein. It can be seen from Fig. 5B that DG based complexes were able to silence GFP expression in cells. In contrast, incubation of cells with the RGD

grafted RDG/shRNA complexes resulted in significantly higher GFP silencing in U-87 MG-GFP cells than complexes based on the HMW 25-kDa PEI. This finding is consistent with fluorescent pictures in Fig. 5A.

To determine the silencing efficiency of the complexes, we counted the percentage of GFP-negative cells using flow cytometry, which showed a similar result as above. As shown in Fig. 5C, silencing achieved by PEI/shRNA complex was as high as 81% due to a high cellular uptake of the complex and the proton sponge effect of PEI [31, 32]. Although RGD peptide was grafted on the RPG/shRNA nanoparticles surface, it had an equivalent silencing efficiency compared with that of DG/shRNA complexes (71%–69%). This result could attribute to the reductive triggered degradation of disulfide-containing DSPEI and subsequent dissociation of DG/shRNA complex in the cellular interior, which helped the shRNA to be released over time and thus a high RNAi efficiency. Moreover, grafting of $\alpha_v\beta_3$ integrin-binding RGD peptide onto DSPEI further enhanced the silencing efficiency (88%) of DG/shRNA, this is mainly due to the efficiently taken up of the complexes by $\alpha_v\beta_3$ integrins-mediated endocytosis. Therefore, with consideration of the above results, RDG can deliver RNA in a tumor cell targeting and reductive intracellular environment controllable way, and thus it could be considered as a very attractive nanotemplate for gene delivery system.

Additionally, the time-dependent RNAi efficiency of RDG/shRNA complexes in U-87 MG-GFP cells was studied. As shown in Fig. 5D, the GNRs-based complexes had maximum RNAi efficiency after the cells were incubated for 42 h, while, in our study, the corresponding time for PEI/shRNA complexes was 48 h. This is mainly because the GSH-triggered delivery process is different from traditional transfection reagents such as PEI and dendrimers. With a transfection reagent, shRNA must slowly dissociate from the transfection reagent, and finally diffuse in the cytosol. For the RGD targeted and GSH-triggered delivery, the GNRs-based complexes can efficiently and quickly uptaken by the target cells and the shRNA is significantly released into the cytosol due to the intracellular GSH-triggered rapid degradation of disulfide-containing DSPEI. Therefore, it is likely that the RNAi efficiency occurs faster due to the integrins receptor mediated endocytosis of the RDG/shRNA and the effecient shRNA release from the GNRs-based complexes in the cytoplasm.

3.6. Biocompatibility of the RDG

In our previous study, the MTT assay against U-87 MG cells indicated that the DSPEI showed significantly lower cytotoxicity than that of PEI-25 kDa, the gold standard of cellular gene transfection reagent. The low cytocompatibility and high cytotoxicity of PEI-25 kDa is probably due to its non-biodegradable nature, high binding and aggregation on the cell surface and internalization, which results in significant necrosis [57]. Since DSPEI is made of the disulfide cross-linked short PEI-1.8 kDa, the disulfide bonds will be cleaved inside cells

due to the high concentration of intracellular GSH. As a result, the high molecular weight DSPEI will be converted into low molecular weight PEIs and hence much lower cytotoxicity. Therefore, DSPEI polycation with low cytotoxicity could be a much safer alternative gene carrier over the PEI-25KDa.

The cytotoxicity of the U-87 MG-GFP cells after incubation with the RDG and PEI 25-kDa delivery vectors were investigated by MTT assay. As shown in Fig. 6A, only 55% of cells were survived when treated with PEI. While, even the concentration of RDG was as high as 25 μg/mL (the concentration above the mass ratio of 5), the cell viability still remained at above 85%, revealing that the RDG had a much lower toxic effect on U-87 MG-GFP cells than PEI 25K. To obtain a more convincing data about the cytotoxicity of RDG, cell viability was determined after the cells were treated with RDG/shRNA complex nanoparticles. As shown in Fig. 6B, the cell viability was more than 80% with RDG/shRNA complex at all tested mass ratios. In contrast, cells treated with non-bioreducible RPG nanoparticles and non-degradable PEI nanoparticles showed the lower cell viability of 65% and 58%, respectively. These results further confirmed that RDG had a much lower cytotoxicity than RPG and PEIs while displayed a higher shRNA transfection efficiency. Therefore, it as appears to be a highly attractive vehicle for shRNA delivery.

3.7. Biodistribution in BALB/c mice

To further investigate the tissue distribution of nanoparticles in an *in vivo* animal model, the GNR-based shRNA complexes were intravenously (i.v.) injected through the tail vein into BALB/c mice bearing U-87 MG-GFP tumors. Major organs including tumors were excised at 12 h after the i.v. injection and ICP-MS was used to analyze quantitatively the Au content contained in the organs and tumors. As shown in Fig. 7, in the case of DSPEI-modified GNR-based complex (DG/shRNA), the gold contents in the tumor was 6.5 % of the total dose, which is likely due to passive targeting via the enhanced permeability and retention (EPR) effect in tumors [58]. The remaining GNRs were found predominantly in the liver and spleen, which is likely due to the high positive charge of DG/shRNA complexes that led to interactions with plasma proteins and cleared by mononuclear phagocyte system (MPS). However, when the GNR PEGylated and modified with RGD peptide, the tissue distribution characteristics of the GNRs were obviously changed. The amount of GNR accumulated in the tumor was significantly higher compared to that of the DG/shRNA group (15.2 v.s. 6.5%), which highlighted the value of RGD modification for targeted tumor accumulation. Notably, the PEGylated RDG/shRNA complex seems to preferentially appear in angiogenesis-related systems, where they show stable circulation in the blood and accumulation in the heart and lung at 12 h post injection. This is mainly due to the coupling of PEG to the composition of the delivery systems, making nanoparticle stealth, can dramatically

prevent or minimize serum protein adsorption and avoid uptake by reticuloendothelial system (RES), so as to prolong their residence time in blood. Besides, both the two groups showed a relative higher GNR accumulation in kidney, indicating possible clearance of these GNRs through the renal system. From the analysis above, we can clearly conclude that the PEGylated DG/shRNA complex could stable and long circulating in the blood [58-60], especially, the nanoparticles can target and accumulate in tumor tissues, which will deliver more RNA to tumor sites and result in a better RNAi efficiency.

3.8. In vivo RNA interference

The fluorescence images of frozen sections of tumors in Fig. 8A and B qualitatively showed the *in vivo* RNAi effect 48 h after U-87 MG-GFP tumors bearing BALB/c mice were injected with GNR-based complexes and PEI/shRNA complexes. The tumors treated with saline control exhibited strong green fluorescence, while the nanoparticle complexes treated groups showed markedly decreased GFP expression in tumors, especially, the RDG/shRNA complex group which showed almost no visible fluorescence (Fig. 8B-d). The quantitative result of RNAi *in vivo* was further detected by using flow cytometry, which corresponded with the *in vitro* RNAi study. As shown in Fig. 8C, GFP silencing efficiency achieved with DG/shRNA complex was about 59%, PEI/shRNA complex revealed a higher efficiency of 72%, and most notably, the RDG/shRNA complex has as high as 82% GFP silenced in tumors. This result is in good agreement with the above biodistribution and cellular release results, where the complexes are effectively accumulated into the tumor by exploiting the EPR effect and efficient RGD-mediated endocytosis. After which the proton-sponge effects of the DSPEI and GSH content triggers endosomal escape and degradation of the DSPEI, allowing for sufficient release of the encapsulated shRNAs into cytoplasm to achieve high RNAi efficiency. For high molecular weight polyethyleneimine (PEI-25KDa) where despite of high efficacy, its high toxicity and cytotoxicity have greatly restricted its applications, especially under *in vivo* conditions [61]. More importantly, despite a great number of studies on nonviral RNA carriers at cellular level, few has demonstrated high efficacy like RDG gene carrier *in vivo*. Therefore, the experimental data shown here suggested that RDG could be a promising non-viral vector for efficient shRNA delivery.

4. Conclusion

In conclusion, RDG could tightly condense shRNAs into stable complex nanoparticles. The RDG/shRNA nanoparticle was found to be highly selective in targeting the U-87 MG-GFP cells with over-expressed $\alpha_v\beta_3$ integrins via receptor-mediated endocytosis. The cleavage of disulfide bonds of DSPEI in the reductive

intracellular environment triggered the degradation of RDG/shRNA complexes and rapid release of shRNAs, contributing to a high RNAi efficiency and low cytotoxicity. Furthermore, their high stability and prolonged blood circulation time allowed for highly efficient tumor tissues accumulation and cell internalization. Consequently, the RDG/shRNA complexes have enabled an outstanding tumor gene silencing efficiency in U-87 MG-GFP tumor bearing BALB/c mice better than that of the PEI/shRNA complex. The RDG/shRNA complex, which combines RGD-mediated active targeting and glutathione-triggered intracellular release and low cytotoxicity, appears to be a highly promising non-viral vector for efficient RNA delivery and therapy. Further work on co-delivery of therapeutic gene and anticancer drugs using this carrier is currently underway in our lab to exploit the synergy of multimodal cancer therapy.

Acknowledgement

This work is supported by National Natural Science Foundation of China (NSFC, Grant No.81171439), National Basic Research Program of China (973 Program, Grant 2010CB529902), the National Key Technology R&D Program of the Ministry of Science and Technology (2012BAI18B01) and the European Research Council via a Marie Curie International Incoming Fellowship to S.G. (grant No: PIIF-GA-2012-331281)

Appendix A. Supplementary data

Supplementary data associated with this article can be found, in the online version, at XXX.

References

[1] Castanotto D, Rossi JJ. The promises and pitfalls of RNA-interference-based therapeutics. Nature 2009;457:426-33.

[2] Whitehead KA, Langer R, Anderson DG. Knocking down barriers: advances in siRNA delivery. Nat Rev Drug Discov 2009;8:129-38.

[3] Arthanari Y, Pluen A, Rajendran R, Aojula H, Demonacos C. Delivery of therapeutic shRNA and siRNA by Tat fusion peptide targeting BCR-ABL fusion gene in Chronic Myeloid Leukemia cells. J Controlled Release 2010;145:272-80.

[4] Davis ME, Zuckerman JE, Choi CH, Seligson D, Tolcher A, Alabi CA, et al. Evidence of RNAi in humans from systemically administered siRNA via targeted nanoparticles. Nature 2010;464:1067-70.

[5] Merritt WM, Bar-Eli M, Sood AK. The dicey role of Dicer: implications for RNAi therapy. Cancer Res 2010;70:2571-4.

[6] Soutschek J, Akinc A, Bramlage B, Charisse K, Constien R, Donoghue M, et al. Therapeutic silencing of an endogenous gene by systemic administration of modified siRNAs. Nature 2004;432:173-8.

[7] Huschka R, Barhoumi A, Liu Q, Roth JA, Ji L, Halas NJ. Gene silencing by gold nanoshell-mediated delivery and laser-triggered release of antisense oligonucleotide and siRNA. Acs Nano 2012;6:7681-91.

[8] Lee JS, Green JJ, Love KT, Sunshine J, Langer R, Anderson DG. Gold, poly(beta-amino ester) nanoparticles for small interfering RNA delivery. Nano Lett 2009;9:2402-6.

[9] Andersen MO, Lichawska A, Arpanaei A, Rask Jensen SM, Kaur H, Oupicky D, et al. Surface functionalisation of PLGA nanoparticles for gene silencing. Biomaterials 2010;31:5671-7.

[10] Cao H, Jiang X, Chai C, Chew SY. RNA interference by nanofiber-based siRNA delivery system. J Controlled Release 2010;144:203-12.

[11] Huh MS, Lee SY, Park S, Lee S, Chung H, Choi Y, et al. Tumor-homing glycol chitosan/polyethylenimine nanoparticles for the systemic delivery of siRNA in tumor-bearing mice. J Controlled Release 2010;144:134-43.

[12] Ganta S, Devalapally H, Shahiwala A, Amiji M. A review of stimuli-responsive nanocarriers for drug and gene delivery. J Controlled Release 2008;126:187-204.

[13] Morille M, Passirani C, Vonarbourg A, Clavreul A, Benoit JP. Progress in developing cationic vectors for non-viral systemic gene therapy against cancer. Biomaterials 2008;29:3477-96.

[14] Taratula O, Garbuzenko OB, Kirkpatrick P, Pandya I, Savla R, Pozharov VP, et al. Surface-engineered targeted PPI dendrimer for efficient intracellular and intratumoral siRNA delivery. J Controlled Release 2009;140:284-93.

[15] Lu W, Zhang G, Zhang R, Flores LG, 2nd, Huang Q, Gelovani JG, et al. Tumor site-specific silencing of NF-kappaB p65 by targeted hollow gold nanosphere-mediated photothermal transfection. Cancer Res 2010;70:3177-88.

[16] Poon L, Zandberg W, Hsiao D, Erno Z, Sen D, Gates BD, et al. Photothermal release of single-stranded DNA from the surface of gold nanoparticles through controlled denaturating and Au-S bond breaking. Acs Nano 2010;4:6395-403.

[17] Huang Y, Lin D, Jiang Q, Zhang W, Guo S, Xiao P, et al. Binary and ternary complexes based on polycaprolactone-graft-poly (N, N-dimethylaminoethyl methacrylate) for targeted siRNA delivery. Biomaterials 2012;33:4653-64.

[18] Yu B, Hsu SH, Zhou C, Wang X, Terp MC, Wu Y, et al. Lipid nanoparticles for hepatic delivery of small interfering RNA. Biomaterials 2012;33:5924-34.

[19] Huang X, El-Sayed IH, Qian W, El-Sayed MA. Cancer cell imaging and photothermal therapy in the near-infrared region by using gold nanorods. J Am Chem Soc 2006;128:2115-20.

[20] Tong L, Zhao Y, Huff TB, Hansen MN, Wei A, Cheng JX. Gold Nanorods Mediate Tumor Cell Death by Compromising Membrane Integrity. Adv Mater 2007;19:3136-41.

[21] Wang CG, Chen Y, Wang TT, Ma ZF, Su ZM. Monodispersed gold nanorod-embedded silica particles as novel Raman labels for biosensing. Adv Funct Mater 2008;18:355-61.

[22] von Maltzahn G, Centrone A, Park JH, Ramanathan R, Sailor MJ, Hatton TA, et al. SERS-Coded Gold Nanorods as a Multifunctional Platform for Densely Multiplexed Near-Infrared Imaging and Photothermal Heating. Adv Mater 2009;21:3175-80.

[23] Chen CC, Lin YP, Wang CW, Tzeng HC, Wu CH, Chen YC, et al. DNA-gold nanorod conjugates for remote control of localized gene expression by near infrared irradiation. J Am Chem Soc 2006;128:3709-15.

[24] Wijaya A, Schaffer SB, Pallares IG, Hamad-Schifferli K. Selective release of multiple DNA oligonucleotides from gold nanorods. Acs Nano 2009;3:80-6.

[25] Cui D, Huang P, Zhang C, Ozkan CS, Pan B, Xu P. Dendrimer-modified gold nanorods as efficient controlled gene delivery system under near-infrared light irradiation. J Controlled Release 2011;152 Suppl 1:e137-9.

[26] Huschka R, Zuloaga J, Knight MW, Brown LV, Nordlander P, Halas NJ. Light-induced release of DNA from gold nanoparticles: nanoshells and nanorods. J Am Chem Soc 2011;133:12247-55.

[27] Majoros IJ, Myc A, Thomas T, Mehta CB, Baker JR, Jr. PAMAM dendrimer-based multifunctional conjugate for cancer therapy: synthesis, characterization, and functionality. Biomacromolecules 2006;7:572-9.

[28] Hauck TS, Ghazani AA, Chan WC. Assessing the effect of surface chemistry on gold nanorod uptake, toxicity, and gene expression in mammalian cells. Small 2008;4:153-9.

[29] Takahashi H, Niidome T, Kawano T, Yamada S, Niidome Y. Surface modification of gold nanorods using layer-by-layer technique for cellular uptake. J Nanopart Res 2008;10:221-8.

[30] Huang HC, Barua S, Kay DB, Rege K. Simultaneous enhancement of photothermal stability and gene delivery efficacy of gold nanorods using polyelectrolytes. Acs Nano 2009;3:2941-52.

[31] Boussif O, Zanta MA, Behr JP. Optimized galenics improve in vitro gene transfer with cationic molecules up to 1000-fold. Gene Ther 1996;3:1074-80.

[32] Akinc A, Thomas M, Klibanov AM, Langer R. Exploring polyethylenimine-mediated DNA transfection and the proton sponge hypothesis. J Gene Med 2005;7:657-63.

[33] Godbey WT, Wu KK, Mikos AG. Size matters: molecular weight affects the efficiency of poly(ethylenimine) as a gene delivery vehicle. J Biomed Mater Res 1999;45:268-75.

[34] Fischer D, Bieber T, Li Y, Elsasser HP, Kissel T. A novel non-viral vector for DNA delivery based on low molecular weight, branched polyethylenimine: effect of molecular weight on transfection efficiency and cytotoxicity. Pharm Res 1999;16:1273-9.

[35] Gosselin MA, Guo W, Lee RJ. Efficient gene transfer using reversibly cross-linked low molecular weight polyethylenimine. Bioconjug Chem 2001;12:989-94.

[36] Neu M, Sitterberg J, Bakowsky U, Kissel T. Stabilized nanocarriers for plasmids based upon cross-linked poly(ethylene imine). Biomacromolecules 2006;7:3428-38.

[37] Wang Y, Chen P, Shen J. The development and characterization of a glutathione-sensitive cross-linked polyethylenimine gene vector. Biomaterials 2006;27:5292-8.

[38] Breunig M, Lungwitz U, Liebl R, Goepferich A. Breaking up the correlation between efficacy and toxicity for nonviral gene delivery. Proc Natl Acad Sci U S A 2007;104:14454-9.

[39] Xu PS, Quick GK, Yeo Y. Gene delivery through the use of a hyaluronate-associated intracellularly degradable crosslinked polyethyleneimine. Biomaterials 2009;30:5834-43.

[40] Saito G, Swanson JA, Lee KD. Drug delivery strategy utilizing conjugation via reversible disulfide linkages: role and site of cellular reducing activities. Adv Drug Deliv Rev 2003;55:199-215.

[41] Schafer FQ, Buettner GR. Redox environment of the cell as viewed through the redox state of the glutathione disulfide/glutathione couple. Free Radic Biol Med 2001;30:1191-212.

[42] Allman R, Cowburn P, Mason M. In vitro and in vivo effects of a cyclic peptide with affinity for the alpha(nu)beta3 integrin in human melanoma cells. Eur J Cancer 2000;36:410-22.

[43] Hood JD, Cheresh DA. Role of integrins in cell invasion and migration. Nat Rev Cancer 2002;2:91-100.

[44] Jiang X, Sha X, Xin H, Chen L, Gao X, Wang X, et al. Self-aggregated pegylated poly (trimethylene carbonate) nanoparticles decorated with c(RGDyK) peptide for targeted paclitaxel delivery to integrin-rich tumors. Biomaterials 2011;32:9457-69.

[45] Li ZM, Huang P, Zhang XJ, Lin J, Yang S, Liu B, et al. RGD-Conjugated Dendrimer-Modified Gold Nanorods for in Vivo Tumor Targeting and Photothermal Therapy. Mol Pharmaceut 2010;7:94-104.

[46] Yang X, Hong H, Grailer JJ, Rowland IJ, Javadi A, Hurley SA, et al. cRGD-functionalized, DOX-conjugated, and (6)(4)Cu-labeled superparamagnetic iron oxide nanoparticles for targeted anticancer drug delivery and PET/MR imaging. Biomaterials 2011;32:4151-60.

[47] Wang FH, Shen YY, Zhang WJ, Li M, Wang Y, Zhou DJ, et al. Efficient, dual-stimuli responsive cytosolic gene delivery using a RGD modified disulfide-linked polyethylenimine functionalized gold nanorod. Journal of Controlled Release 2014;196:37-51.

[48] Jiang XL, Liu J, Xu L, Zhuo RX. Disulfide-Containing Hyperbranched Polyethylenimine Derivatives via Click Chemistry for Nonviral Gene Delivery. Macromol Chem Phys 2011;212:64-71.

[49] Yin Q, Gao Y, Zhang Z, Zhang P, Li Y. Bioreducible poly (beta-amino esters)/shRNA complex nanoparticles for efficient RNA delivery. J Controlled Release 2011;151:35-44.

[50] Koping-Hoggard M, Varum KM, Issa M, Danielsen S, Christensen BE, Stokke BT, et al. Improved chitosan-mediated gene delivery based on easily dissociated chitosan polyplexes of highly defined chitosan oligomers. Gene Ther 2004;11:1441-52.

[51] Lee Y, Lee SH, Kim JS, Maruyama A, Chen X, Park TG. Controlled synthesis of PEI-coated gold nanoparticles using reductive catechol chemistry for siRNA delivery. J Controlled Release 2011;155:3-10.

[52] Shim MS, Kwon YJ. Stimuli-responsive polymers and nanomaterials for gene delivery and imaging applications. Adv Drug Deliv Rev 2012;64:1046-59.

[53] Wang L, Jin Y, Deng J, Chen G. Gold nanorods-based FRET assay for sensitive detection of Pb2+ using 8-17DNAzyme. Analyst 2011;136:5169-74.

[54] Zeng Q, Zhang Y, Liu X, Tu L, Kong X, Zhang H. Multiple homogeneous immunoassays based on a quantum dots-gold nanorods FRET nanoplatform. Chem Commun (Camb) 2012;48:1781-3.

[55] Ghosh PS, Kim CK, Han G, Forbes NS, Rotello VM. Efficient Gene Delivery Vectors by Tuning the Surface Charge Density of Amino Acid-Functionalized Gold Nanoparticles. Acs Nano 2008;2:2213-8.

[56] Levy EJ, Anderson ME, Meister A. Transport of Glutathione Diethyl Ester into Human-Cells. Proc Natl Acad Sci U S A 1993;90:9171-5.

[57] Liu J, Jiang X, Xu L, Wang X, Hennink WE, Zhuo R. Novel reduction-responsive cross-linked polyethylenimine derivatives by click chemistry for nonviral gene delivery. Bioconjug Chem 2010;21:1827-35.

[58] Wang Y, Black KC, Luehmann H, Li W, Zhang Y, Cai X, et al. Comparison study of gold nanohexapods, nanorods, and nanocages for photothermal cancer treatment. Acs Nano 2013;7:2068-77.

[59] Oe Y, Christie RJ, Naito M, Low SA, Fukushima S, Toh K, et al. Actively-targeted polyion complex micelles stabilized by cholesterol and disulfide cross-linking for systemic delivery of siRNA to solid tumors. Biomaterials 2014;35:7887-95.

[60] von Maltzahn G, Park JH, Agrawal A, Bandaru NK, Das SK, Sailor MJ, et al. Computationally guided photothermal tumor therapy using long-circulating gold nanorod antennas. Cancer Res 2009;69:3892-900.

[61] Godbey WT, Wu KK, Mikos AG. Size matters: molecular weight affects the efficiency of poly(ethylenimine) as a gene delivery vehicle. J Biomed Mater Res 1999;45:268-75.

Figure Captions:

Fig. 1. Characterization of RDG/shRNA complexes. (A) Agarose gel electrophoresis photos of RDG/shRNA complexes at different mass ratios. (B) shRNA binding efficiency and (C) Zeta potentials of the complexes at various mass ratios. Error bars represent standard deviations (n = 4). (D) A TEM image of RDG/shRNA complexes at a mass ratio of 5. Mass ratios means the weight ratio of the GNR nanocarriers to GFP-shRNA.

Fig. 2. *In vitro* GSH-triggered shRNA release from RDG/shRNA complexes. (A) Gel retardation analyses of RDG/shRNA complexes at various mass ratios in the presence of 3 mM GSH. (B) percents of shRNA released from RDG/shRNA complexes in the presence of 3 mM GSHfor 30 min. Error bars represent standard deviations (n = 3). Mass ratios means the weight ratio of the GNR nanocarriers to GFP-shRNA.

Fig. 3. Tumor cell targeting of RDG/shRNA complexes. (A) Dark-field images of MCF-7 cells incubated with RDG/shRNA (a), U-87 MG-GFP cells incubated with DG/shRNA (b), U-87 MG-GFP cells incubated with RDG/shRNA (c) and U-87 MG-GFP cells incubated with 1 mM free RGD and RDG/shRNA (d). (B) Quantification of the mean GNR number per cell determined by ICP-MS of (a), (b), (c) and (d). Data are presented as mean ± SD (n = 3). ** :$P < 0.01$.

Fig. 4. Intracellular GSH-triggered release of shRNA from GNR-based complexes in U-87 MG cells. (A) Flow cytometry histogram profile of U-87 MG cells incubated with RPG/shRNA and RDG/shRNA complexes. The

cells were pre-treated with GSH-OEt for 2 h to determine the influence of intracellular GSH on the release of shRNA from the complexes. (B) Intracellular mean fluorescence intensity of in U-87 MG cells treated with RPG/shRNA and RDG/shRNA complexes. (C) Confocal laser scanning microscope images of U-87 MG cells treated with RDG/shRNA. The cells were pre-treated without (a) or with (b) 10 mM GSH-OEt for 2 h. Blue: Hoechst 33342 stained nucleus; green: YOYO-1 labeled shRNA; red: Lyso-tracker red stained lysosome. Data are presented as mean ± SD. **: $P < 0.01$ is considered significantly difference.

Fig. 5. *In vitro* RNAi experiment. (A) Fluorescent pictures of RNAi, (B) GFP fluorescence quantitative analysis (Results are shown as relative light units (RLU)/mg of protein.) and (C) GFP silencing efficiency of PEI/shRNA complex at N/P of 10, DG/shRNA complex, RPG/shRNA complex or RDG/shRNA complex at mass ratio of 5 in U-87 MG-GFP cells. Negative control of untreated cells. Cells were incubated with complexes for 4 h, followed by further culture of 42 h for the GNRs-based complexes or 48 h for the PEI/DNA complex. (D) Time-dependent GFP silencing efficiency of PEI/shRNA and RDG/shRNA complex complexes in U-87 MG-GFP cells. Data displayed as mean ± SD (n = 3). * :$P < 0.05$, **:$P < 0.01$. $P < 0.05$ is considered significantly difference.

Fig. 6. Cell viability determined by MTT assay. (A) Cytotoxicity of RDG at concentrations of 1, 5, 25, 50 and 75 μg/mL against U-87 MG-GFP cells.PEI 25-kDa at the concentration of 3.9 μg/ml (the concentration of PEI 25-kDa at N/P ratio of 10) was set as positive control. (B) Cytotoxicity of RDG/shRNA complex at mass ratios of 10, 7.5 and 5, RPG/shRNA complex at a mass ratio of 5 and PEI/shRNA complex at a N/P ratio of 10 with shRNA concentration of 3 μg/mL against U-87 MG-GFP cells. Data displayed as mean ± SD (n = 5). *:$P < 0.05$, **:$P < 0.01$ compared with PEI group.

Fig. 7. *In vivo* biodistributions of the DG/shRNA and RDG/shRNA complexes at 12 h after intravenous injection in tumor-bearing mice. The amounts of Au invarious tissues or organs were analyzed by ICP-MS. Error bars are standard errors with n = 5. *:$P < 0.05$, **:$P < 0.01$ compared with the other group.

Fig. 8. *In vivo* RNAi experiment. (A) Representative fluorescence images of the tumors harvested from BALB/C mice bearing U-87 MG-GFP tumors at 48 h after intravenous injection of saline, PEI/shRNA complex, DG/shRNA complex and RDG/shRNA complex. (B) Frozen sections of tumors taken out from BALB/C mice treated with saline, PEI/shRNA complex, DG/shRNA complex and RDG/shRNA complex. (C) Quantitative analyses of intra-tumor GFP silencing efficiency in BALB/c mice bearing U-87 MG-GFP tumor of PEI/shRNA complex, DG/shRNA complex and RDG/shRNA complex by flow cytometry.

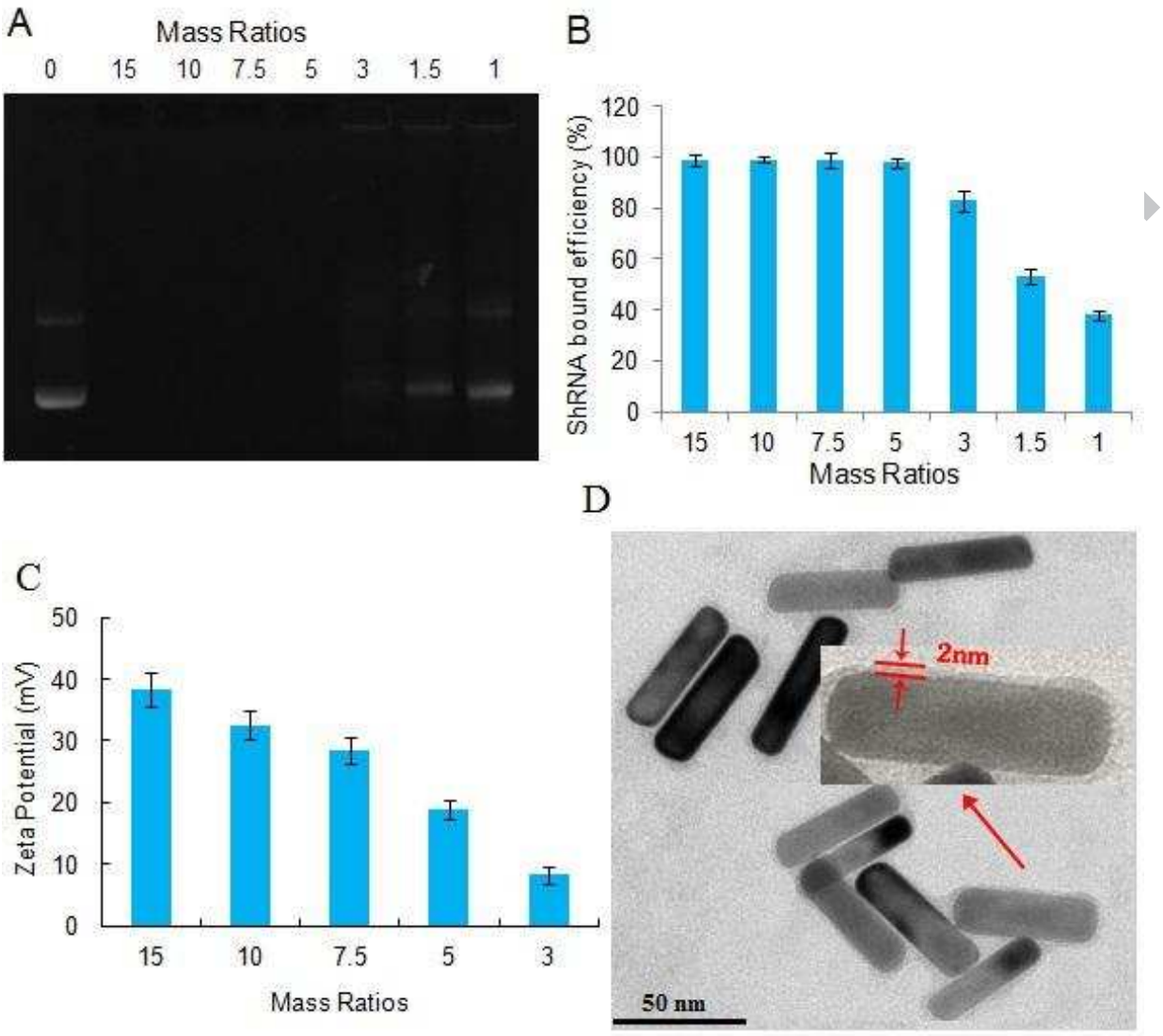

Fig. 1.

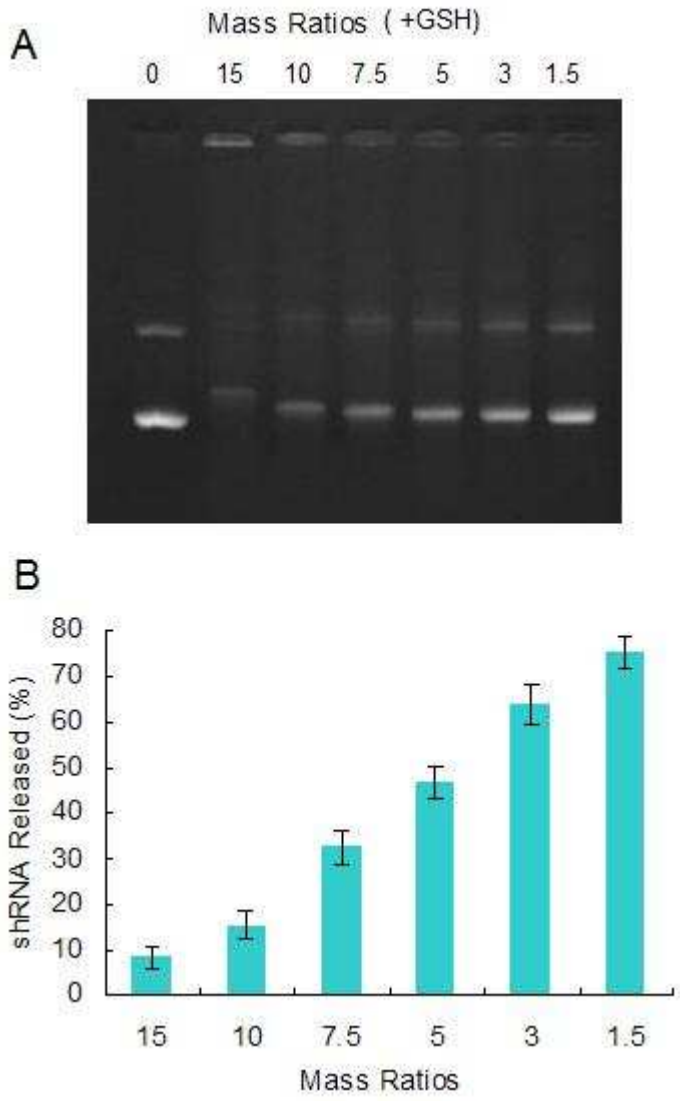

Fig. 2.

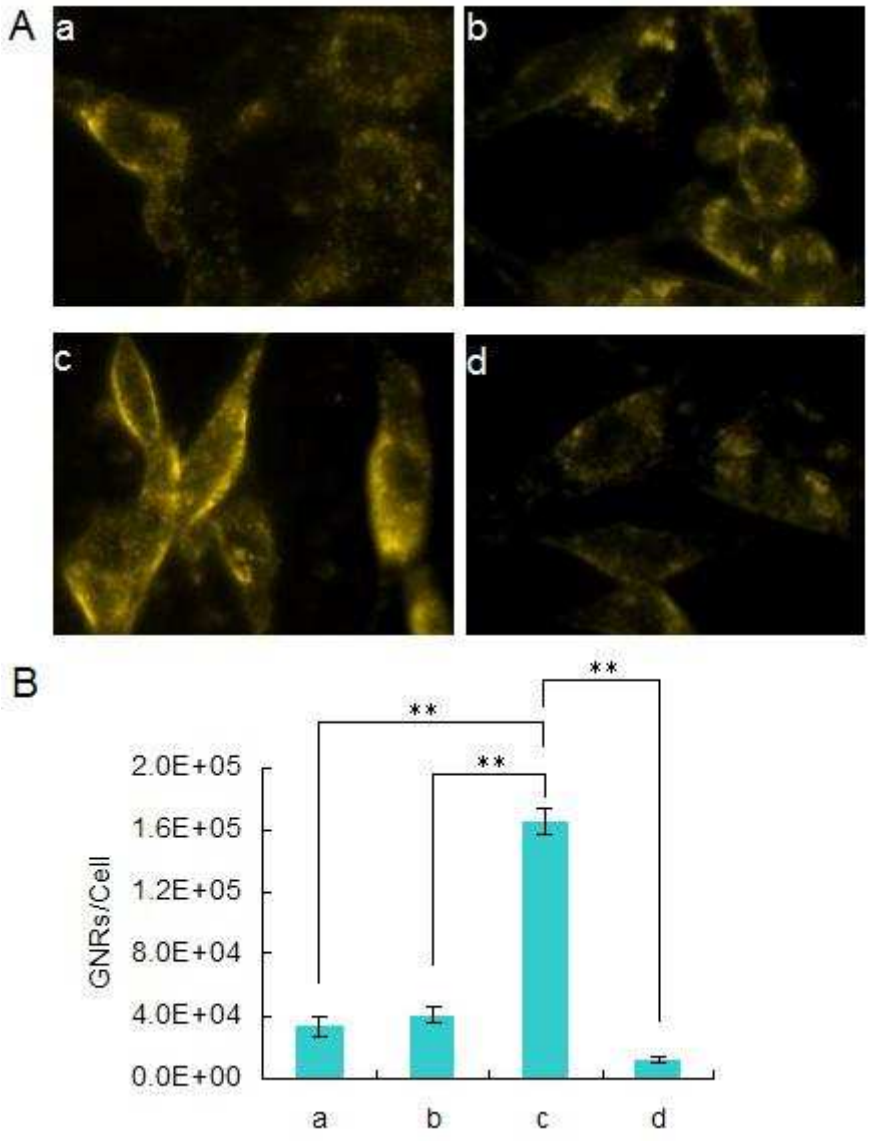

Fig. 3.

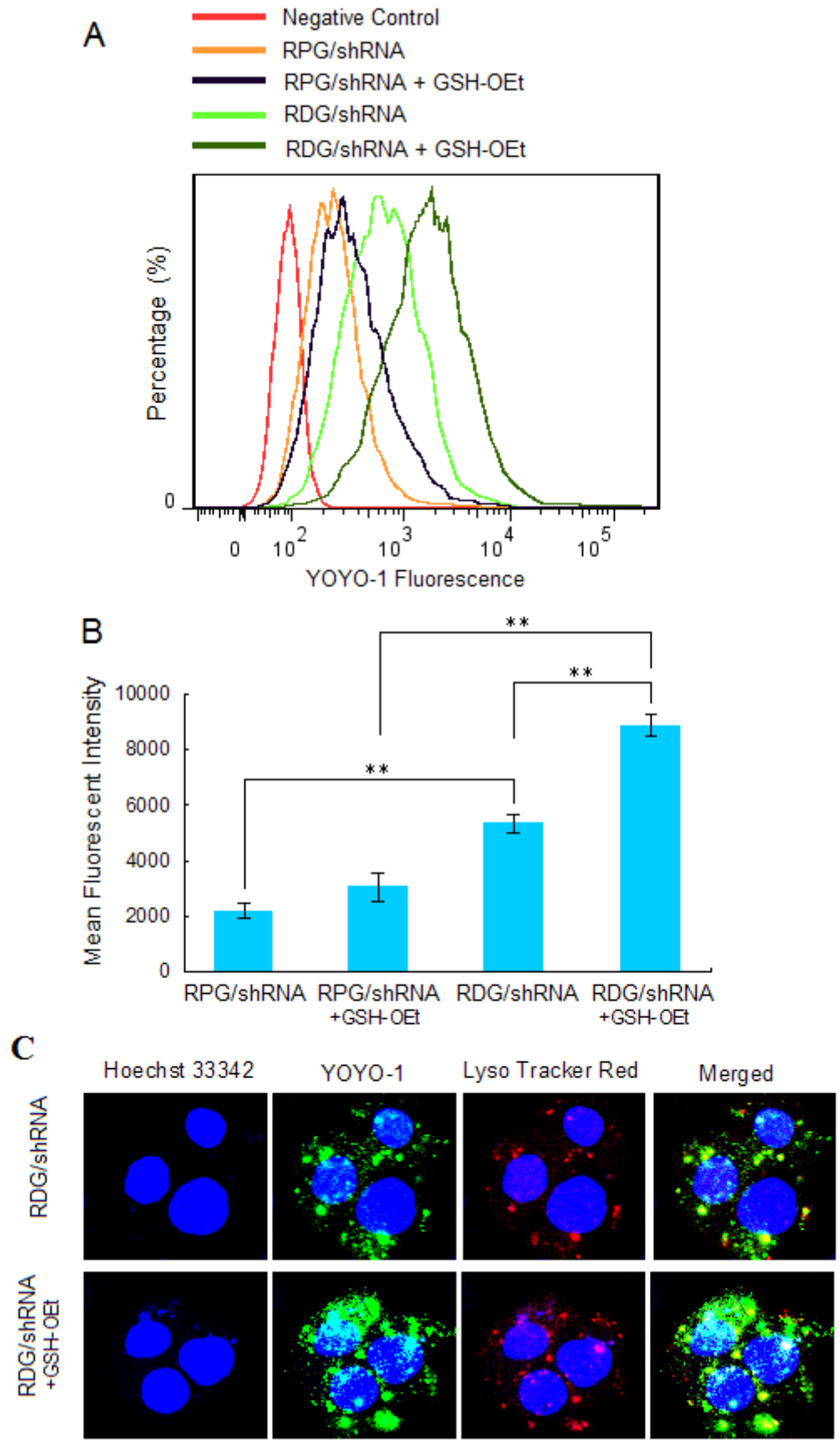

Fig. 4.

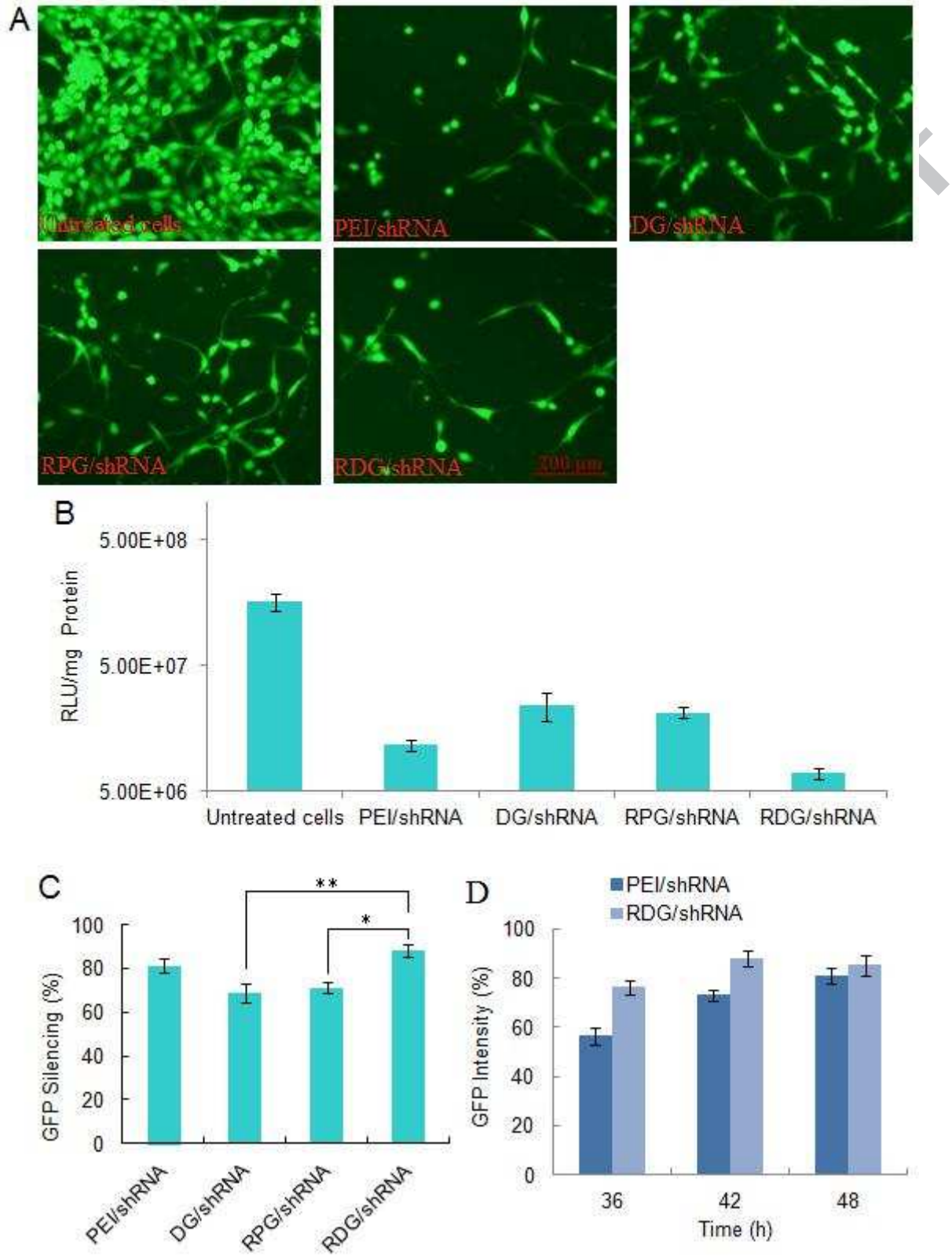
A
Untreated cells
PEI/shRNA
DG/shRNA
RPG/shRNA
RDG/shRNA
200 μm
B
RLU/mg Protein
5.00E+08
5.00E+07
5.00E+06
Untreated cells
PEI/shRNA
DG/shRNA
RPG/shRNA
RDG/shRNA
C
GFP Silencing (%)
100
80
60
40
20
0
**
*
PEI/shRNA
DG/shRNA
RPG/shRNA
RDG/shRNA
D
PEI/shRNA
RDG/shRNA
GFP Intensity (%)
100
80
60
40
20
0
36
42
48
Time (h)

Fig. 5.

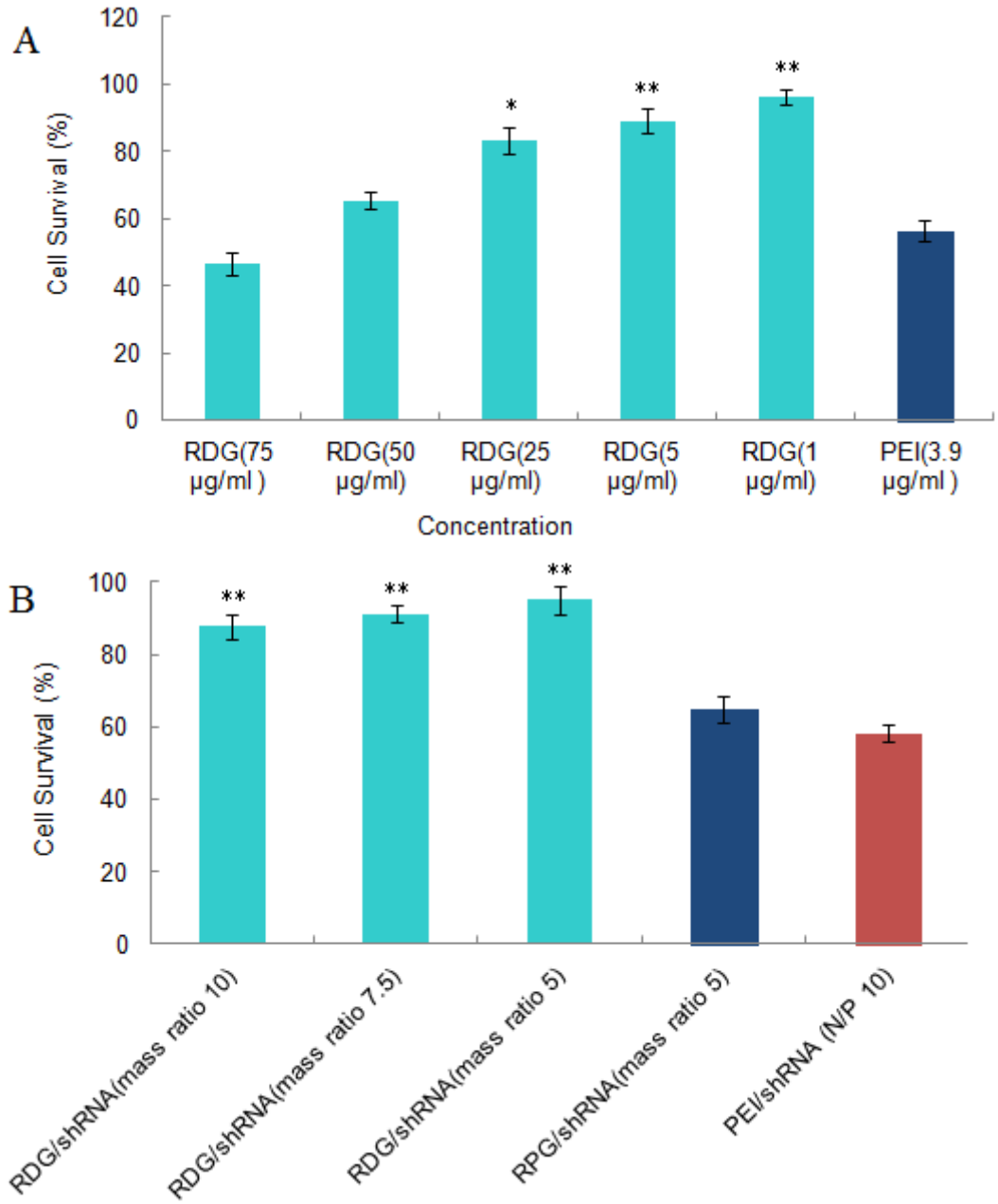

Fig. 6.

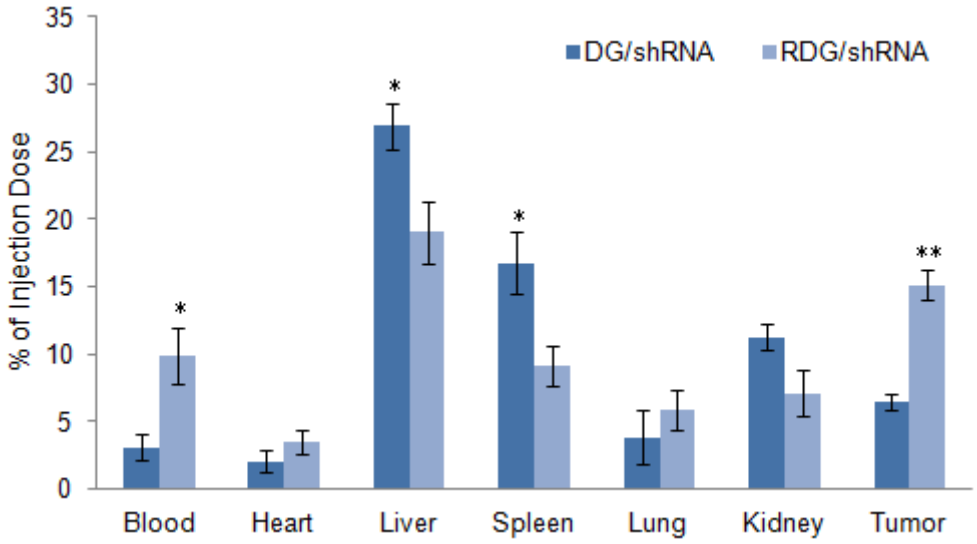

Fig. 7.

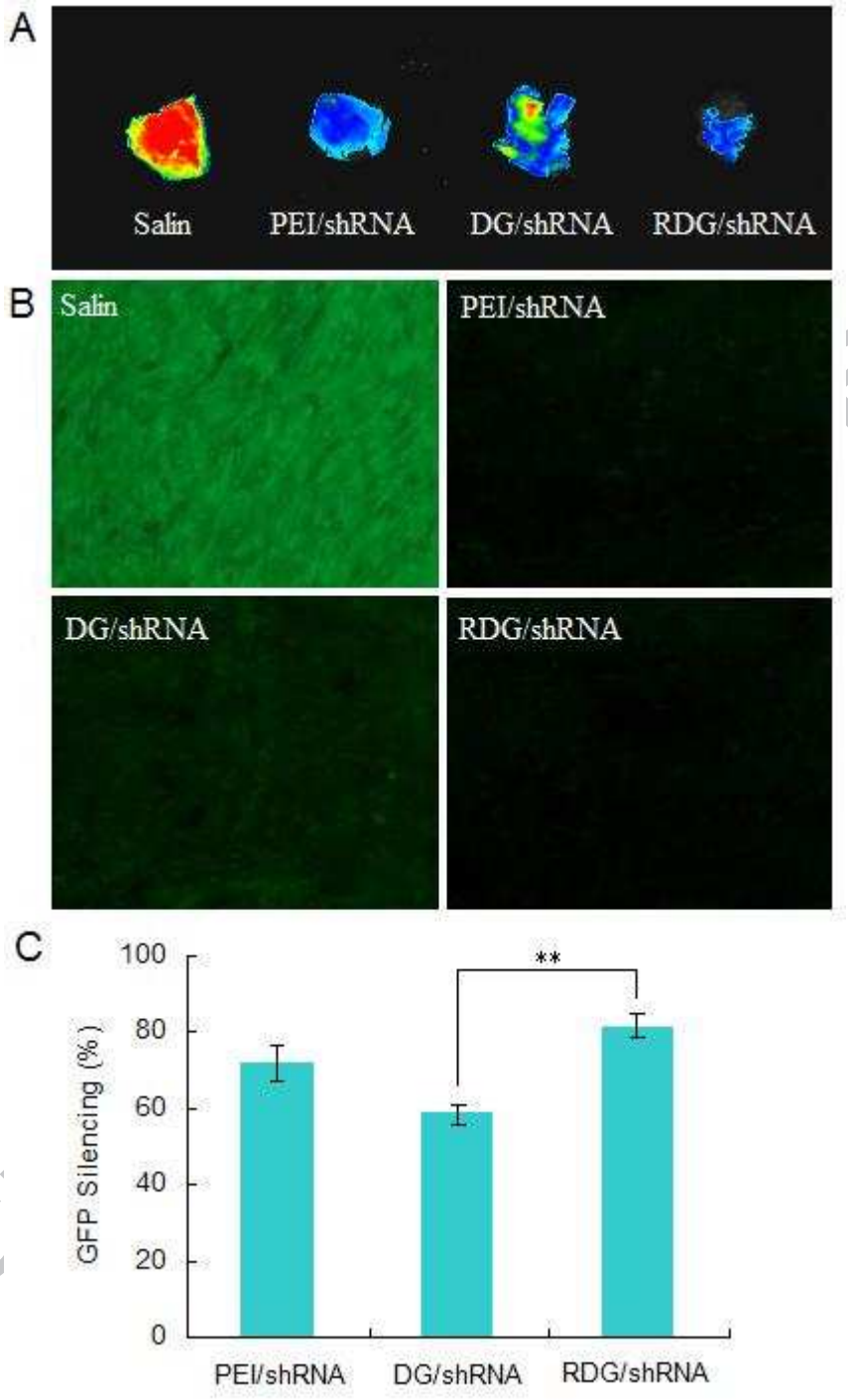

Fig. 8.

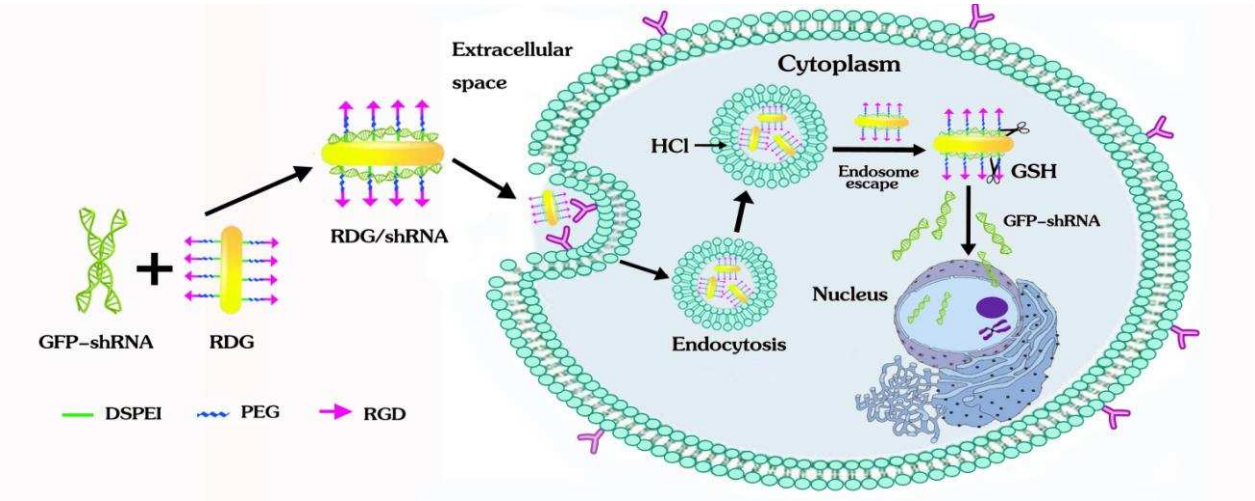

Graphical Abstract